INSTITUT DE FRANCE
Académie des sciences

Comptes Rendus

Mécanique

Thomas Ackermann, Sami Kaidi, Philippe Sergent and Emmanuel Lefrançois

Development of a polar-based method for the calculation of the leeway of floating objects drifting at sea

Volume 350 (2022), p. 431-450

Published online: 6 September 2022

https://doi.org/10.5802/crmeca.125

Les Comptes Rendus. Mécanique *sont membres du Centre Mersenne pour l'édition scientifique ouverte*
www.centre-mersenne.org
e-ISSN : 1873-7234

Comptes Rendus
Mécanique
2022, Vol. 350, p. 431-450
https://doi.org/10.5802/crmeca.125

Short paper / *Note*

Development of a polar-based method for the calculation of the leeway of floating objects drifting at sea

Développement d'une méthode de calcul de la dérive des objet flottants en mer basée sur l'utilisation de polaires

Thomas Ackermann *, [a], **Sami Kaidi** [a], **Philippe Sergent** [a] and **Emmanuel Lefrançois** [b]

[a] CEREMA Risques, Eau et Mer, Equipe Projet Recherche Hydraulique pour l'Aménagement, Margny-lès-Compiègne, France

[b] UTC, Compiègne, France

E-mails: thomas.ackermann@cerema.fr (T. Ackermann), sami.kaidi@cerema.fr (S. Kaidi), philippe.sergent@cerema.fr (P. Sergent), emmanuel.lefrancois@utc.fr (E. Lefrançois)

Abstract. Localisation of drifting objects and lost at sea persons is an integral part of search and rescue (SAR) missions. It is thus important to possess effective tools to determine the trajectory of such objects. The method currently used presents some limitations and may prove imprecise in certain cases. The development of a new method based on CFD-generated drag and lift polars is therefore investigated as an alternative. This approach is implemented in a simplified manner for a 40-feet container, and the results compared to the method currently in use. These results, though improvable, appear promising and prove the potential of this approach.

Résumé. La localisation des objets flottants et des personnes à la dérive est une part importante des missions de sauvetage en mer, il est dès lors important de disposer d'outils efficaces pour déterminer la trajectoire de tels objets. La méthode actuellement employée présente certaines limitations et peut s'avérer imprécise. Le développement d'une nouvelle méthode basée sur l'utilisation de polaires de coefficients aérodynamiques calculés à l'aide d'outils de mécanique des fluides numérique est considéré en tant qu'alternative. Cette approche est mise en œuvre pour un conteneur standard. Ces premiers résultats bien que perfectibles semblent prometteurs et témoignent du potentiel de cette approche.

Keywords. CFD, Leeway, Leeway drift, Polar curve, Search and rescue.

Mots-clés. MFN, Dérive, Méthode du Leeway, Polaires, Recherche et sauvetage.

2020 Mathematics Subject Classification. 76-10.

* Corresponding author.

Manuscript received 3 February 2022, revised 20 June 2022, accepted 18 July 2022.

1. Introduction

Floating objects drifting at sea encompass a wide variety of cases ranging from person in water, oil spill and shipping containers to life raft and other types of craft [1]. Depending on their nature, they may warrant search and rescue (SAR) operations if lives are in jeopardy or if they pose a serious threat to either the safety of ship traffic or to the environment. As such, conducting SAR operations is an integral part of the mission of Maritime Rescue Coordination Center (MRCC) around the globe.

The most recent SAR operational models such as MOTHY (Modèle Océanique de Transport d'Hydrocarbures) for the French MRCC [1], CANSARP (Canadian Search and Rescue Planning Program) for the Canadian Coast Guards [2] and SAROPS (Search and Rescue Optimal Planning System) for the United States Coast Guards [3] make use of environmental data (namely wind and current) stemming from prediction models and object-specific drift properties obtained by the "leeway field method" [4] in order to compute drift trajectories which are then combined through stochastic methods in order to generate a search area. For more details regarding SAR history or forcing fields see [5].

Although the leeway field method has been improved over the years by the introduction of a rigorous definition, the decomposition in downwind and crosswind leeway, and the advent of the "direct method" permitted by improving measurement devices [6, 7], it still remains tainted by uncertainties which are then passed onto the SAR model. This can result in incorrect or rapidly expanding search area, especially considering that SAR models are also subject to uncertainties from current and wind fields.

In this paper we will present a new method to determine drift properties of floating objects using CFD-generated polar coefficients (hereafter referred to as the "polar-based method") and compare it to the leeway field method on a 40-ft shipping container.

Section 2 presents a definition of the leeway and a brief overview of the leeway field method as well as the method to determine a search area. It also provides a brief summary of the shortcoming of these methods. Section 3 describes the proposed polar coefficients-based method and its application to the 40-ft container. Section 4 presents results hailing from the polar-based method and discuss them in regard to existing literature.

2. Leeway and the leeway field method

2.1. *Principle of the leeway*

We will retain in the rest of this work the definition of leeway given by Allen and Plourde in 1999 [6] and illustrated in Figure 1(a):

Leeway is the motion of the object induced by wind (10 m reference height) and waves relative to the ambient current (between 0.3 and 1.0-m depth).

Historically, leeway was expressed by its norm L and the angle to wind (or leeway angle) L_α. The decomposition in its downwind DWL and crosswind CWL components as presented in Figure 1(b) is now preferred as it appears more accurate [7]. Unlike the DWL which has a fixed direction, the CWL has two possible directions. A leeway to the "right" of the downwind direction is designated as positive and a leeway to the "left" of the downwind direction is designated as negative. A sudden change in the sign of the CWL is possible and called a "jibe" [8].

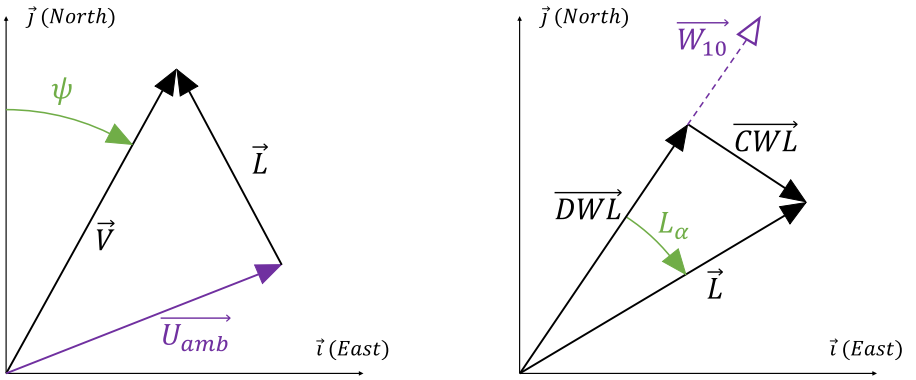

Figure 1. Definition and decomposition of the leeway. (a) Relationship between ship's speed $\vec{V}$, ambient current $\vec{U_{\text{amb}}}$ and leeway $\vec{L}$. (b) Decomposition of the leeway $\vec{L}$ into its downwind $D\vec{W}L$ and crosswind $C\vec{W}L$ component.

The norm of the leeway and its components is assumed to depend linearly on the wind measured 10 m above water W_{10} [4] which results in (1) and (2).

$$DWL = a_D \cdot W_{10} + b_D \tag{1}$$

$$CWL = a_C \cdot W_{10} + b_C. \tag{2}$$

The aim of the leeway field method is to determine the dimensionless leeway coefficients a_D and a_C and the offset coefficients (in m·s^{-1}) b_D and b_C as well as their respective uncertainties.

2.2. *Application*

2.2.1. *The leeway field method*

The leeway field method relies on field experiments where the object whose leeway coefficients are to be determined is put adrift and subsequently monitored to determine its coordinates as well as the ambient current and wind. The speed of the object relative to the surface current is determined from the reading of the trajectory and the ambient current. This relative speed is then compared to the wind speed and the various leeway coefficients are obtained by linear regression [9].

Two different approaches have been used in the leeway field studies [6], described as the "indirect" and "direct" methods based on the way the ambient current was determined. While the indirect method made use of current drifters to estimate the ambient current, the direct method uses current sensors directly attached to the studied object. Due to its higher precision, the direct method has supplanted the indirect method [5]. For more details regarding the leeway field method see [4].

2.2.2. *Determination of a search area*

SAR operational models use a Monte-Carlo-based simulator to generate a probability distribution for the object's location. This probability distribution is the result of the superposition of different weighted scenarios; each scenario corresponding to the simulation of several thousand particles [3].

The simplest drift scenario is defined by the last known position and the associated time. The position and the position uncertainty are used to create a bivariate normal distribution for the

starting position of the drift and a normal distribution is also made for the starting time. Random draws are then made to determine where and when each particle starts its drift.

The velocity of the particle is then equal to the sum of the current velocity and the leeway. The current velocity at the particle location for each time step is derived from the environmental data and a perturbation is added in the form of a random draw from a normal distribution. The downwind and crosswind leeway vary linearly with the wind velocity, which is obtained from the environmental data. The downwind and crosswind slope are set once for each particle via a random draw accounting for standard deviation in the leeway coefficients.

The initial crosswind leeway direction is random, and a jibe probability is added with an exponential law. If the crosswind leeway is important and the jibe probability is low, two high probability areas can appear in the distribution depending on the initial direction of the CWL [7]. Jibing is a complex phenomenon for which data are scarce [10], but it is important in SAR models as it can alter the search area in a significant way [11].

2.3. *Shortcoming*

In addition to a high cost resulting from the need to conduct a measurement campaign at sea, this method is subject to many uncertainties, especially on the measurement of current. The draught can vary greatly between objects, ranging from less than a meter for a life raft to more than 10 m for large cargo ships. Since the current can vary greatly in the first meter of the ocean due to wind and wave-induced current, the value chosen for the reference current is critical, especially for objects with either an extremely shallow draught (less than 0.3 m) or particularly deep draught (more than 10 m). This can lead to strong uncertainties during the linear regression, with correlation coefficients that can be inferior to 0.5, especially for the CWL [8].

It also has to be noted that a wide range of weather conditions will lead to more robust results. However, since trials are conducted in a specific area at a specific time, they may not always cover a wide range of conditions.

Furthermore, this method accounts only indirectly for inertia. The leeway coefficients represent a mean over the duration of the field trial which includes steady and unsteady phase, but the object is thus supposed to be always at equilibrium. For large objects which are slower to reach equilibrium, this could induce higher uncertainties for short drift durations.

Finally, the initial heading is not accounted for but it could permit to determine the initial sign of the CWL. Although the initial heading is only available for ships fitted with Automatic Identification System (AIS), it may in certain case have a significant impact on the probability distribution, thus avoiding the existence of two distinct high probability areas.

3. Polar-based method

We will now present the polar-based method and apply it to a 40-ft shipping container (12.192 m length by 2.438 m breadth by 2.591 m height). This object has been chosen because it has been frequently studied by the leeway field method [8, 9]. It also presents interesting geometric properties which will make the study easier.

The polar-based method does not focus on determining the leeway directly, but rather on determining the object's speed, heading and course. This is done using Newton's second law of motion.

This approach to estimate the leeway has been done previously by Daniel *et al.* for a container [12]. However they considered that the lift force was negligible and did not account for the impact of the angle of incidence of the wind and current.

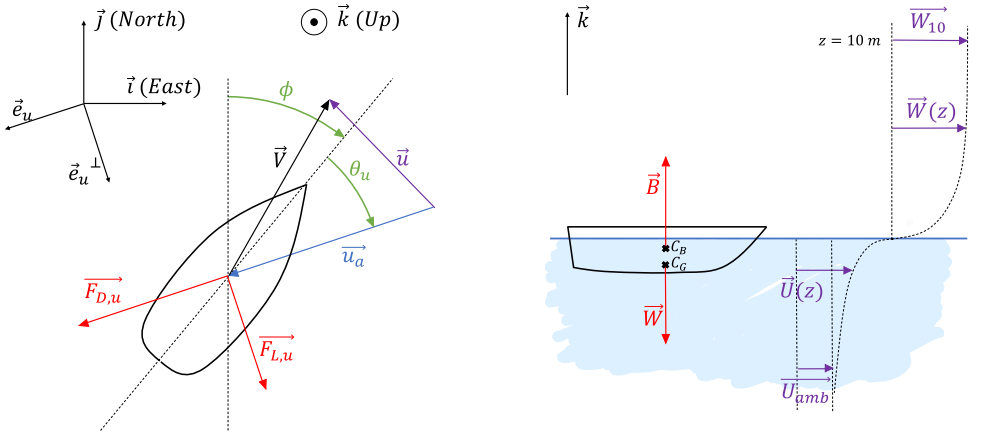

Figure 2. Overview of the forces exerted on the system and meteorological parameters. (a) Relationship between the ship's speed $\vec{V}$ and heading ϕ, and the fluid's true speed $\vec{u}$, apparent speed $\vec{u_a}$ and angle of incidence θ_u. The frame of reference $(\vec{e}_u, \vec{e}_u^{\perp}, \vec{k})$, relative to the fluid is introduced as well as the drag force $\vec{F_{D,u}}$ and lift force $\vec{F_{L,u}}$. (b) The wind $\vec{W}$ and current $\vec{U}$ profile are presented as well as their relationship with the 10-m wind $\vec{W}_{10}$ and ambient current $\vec{U}_{\text{amb}}$. In general these vectors are not collinear. The ship's centre of buoyancy C_B and centre of gravity C_G are also depicted, along with the associated buoyancy force $\vec{B}$ and weight force $\vec{P}$.

3.1. *Theory*

3.1.1. *Forces involved*

We will consider $\sum \vec{F}$ the sum of forces, $\sum \vec{T}$ the sum of torques, m the mass of the object, J its moment of inertia, $\vec{a}$ the acceleration and $\vec{\alpha}$ the angular acceleration. Newton's second law can then be broken into translational terms (3) and rotational term (4).

$$\sum \vec{F} = m\vec{a} \tag{3}$$

$$\sum \vec{T} = J\vec{\alpha}. \tag{4}$$

The forces exerted on the object are its weight $\vec{P}$, the buoyant force $\vec{B}$, the Coriolis force and the forces generated by the action of the wind on the emerged part, by the current on the immersed part, and by the waves [13].

As the object is floating, the weight and the buoyant force cancel each other (see Figure 2b). The Coriolis force is considered as negligible on the study scale in regard to the other forces. The influence of waves can be divided into the wave-induced currents or Stokes drift and the wave forcing on the object [14]. The wave forces acting on the object will not be considered as they are negligible for objects less than 30 m in length [10]. This is also the case for most models [5], even though formulas regarding the drift velocity in waves have been proposed by Le Boulluec *et al.* [15]. We will however try to account for the wave-induced currents by including the Stokes drift.

For simplification, it was decided to neglect pitch, roll and heave. The movement is thus reduced to three degrees of freedom: translation along the axes i and j and rotation around the k axis.

As a result, the only forces being applied on the system are those resulting from the direct action of the wind and current on the object. We will thus adopt the standard decomposition into

a drag force and a lift force. Contrary to what is observed in the case of airplanes, the lift force is not oriented vertically but rather horizontally. This is common when dealing with sails [16].

After this decomposition we are left with four forces and two torques (5), (6). They are as follows: the drag force on the emerged part $\vec{F}_{D,\text{air}}$, the drag force on the immersed part $\vec{F}_{D,\text{water}}$, the lift force on the emerged part $\vec{F}_{L,\text{air}}$, the lift force on the immersed part $\vec{F}_{L,\text{water}}$, the resulting torque on the emerged part $\vec{T}_{\text{air}}$ and the resulting torque on the immersed part $\vec{T}_{\text{water}}$.

$$\sum \vec{F} = \vec{F}_{D,\text{air}} + \vec{F}_{D,\text{water}} + \vec{F}_{L,\text{air}} + \vec{F}_{L,\text{water}} \tag{5}$$

$$\sum \vec{T} = \vec{T}_{\text{air}} + \vec{T}_{\text{water}}. \tag{6}$$

We will use the general formulation of a drag or lift force (7). The fluid density ρ will be taken equal to 1.289 kg·m^{-3} for the emerged part and 1025 kg·m^{-3} for the immersed part. The speed of the object relative to the fluid u_a (see Figure 2a) will be either the apparent wind or the apparent current. The cross-sectional area S and drag or lift coefficient C will depend on the object and its immersion rate.

$$F = \tfrac{1}{2}\rho SC|\vec{u}_a|^2. \tag{7}$$

By analogy we will use the same formula for the torque (8). In this case however a characteristic length l has to be added to keep C dimensionless. This characteristic length was set to 6.096 m, or half the length of a 40-ft container.

$$T = \tfrac{1}{2}\rho SlC|\vec{u}_a|^2. \tag{8}$$

As denoted in Figure 2(b), $\vec{u}_a$ depends on the height z. This prompts us to introduce simplified formula for the wind and the current profile that will be developed in Section 3.1.2. Furthermore, as denoted in Figure 2(a) the drag, the lift and the torque depend on the angle of incidence of the flow θ_u. As such, we will have to use polars of drag, lift and torque coefficient, which we will introduce in Section 3.1.3. Finally, the cross-sectional area also varies depending on θ_u. For simple geometries it is not an issue, but for more complicated objects it may be advisable to directly compute a dimensional coefficient.

3.1.2. *Wind profile and surface current*

Our method requires both a wind profile and a current profile, as there can be significant variations in speed close to the air–water interface due to shearing. However, the leeway field method only takes into account the wind measured at 10 m above water (W_{10}), which is the standard for wind model, and the current measured somewhere between 0.3 and 1 m. In order to make comparisons we have thus to determine a wind and a current profile using only these two parameters.

We implement a logarithmic wind profile $W(z)$ in order to take into account the friction with the ocean surface [17]. We thus have equation (9) with z_0 the roughness coefficient of the sea surface.

$$W(z) = W_{10}\frac{\ln\left(\frac{z}{z_0}\right)}{\ln\left(\frac{10}{z_0}\right)}. \tag{9}$$

There are several formulas to calculate z_0, in particular Charnok's formula [17] but these formulas all require information on the sea state which we do not have in the simulation. We will therefore take $z_0 = 0.00002$ as an average value for an open sea.

For the current profile, we consider an ambient current which is constant over the immersion depth and corresponds to the current used in the leeway method and we add the surface current generated by the force of the wind. As such, $\vec{U} = \vec{U}_{\text{ambient}} + \vec{U}_{\text{surface}}$. The surface current generated by the wind can be further decomposed into the Stokes current and the Lagrangian current [18]. The Lagrangian current being relatively constant over the typical depth of the draft of the objects

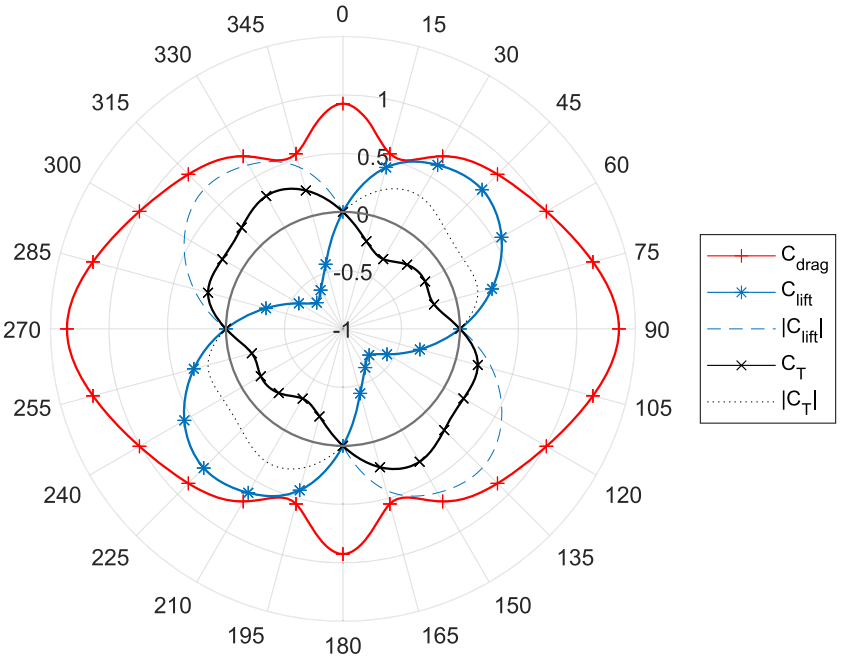

Figure 3. Dimensionless polar of coefficients for a 40-ft container.

considered, it will be counted as being part of the ambient current. We are thus left with the Stokes current which decreases sharply with depth and can have an impact greater than wind drag on a surface drifter [19]. In order to keep the model relatively simple, we use the following equation (10) given by Kenyon [20].

$$U_{\text{surface}}(z) = 3.58.10^{-2} W(19.5) \mathrm{e}^{\frac{-3.93(gz)^{1/2}}{W(19.5)}}. \tag{10}$$

The surface current $\vec{U}_{\text{surface}}$ has the same orientation as the wind $\vec{W}$, but not in general the ambient current. As a result, the orientation of the global current $\vec{U}$ varies depending on the depth z.

3.1.3. *Polars*

The numerical model used in this study was developed considering previous work by Kaidi *et al.* [21] and Razgallah *et al.* [22].

The container was modelled as a parallelepiped with a length of 12.192 m, a height of 2.591 m, and a width of 2.438 m. The container was placed within a larger domain of fluid to avoid the influence of boundaries. For limit condition we applied a velocity inlet with a unitary value of 1 m·s^{-1} and a pressure outlet, the other boundaries (sides, bottom and top) were set as symmetry conditions. Tests were performed using the StarCCM+ software by solving the steady Navier–Stokes equation. To reduce computation time the free surface was neglected and the container was supposed completely emerged. Polars were determined by rotating the container over 360° with a 15° step. As a unitary velocity was used, dimensionless coefficients are then directly obtained considering the fluid density ρ and the projected surface S.

The drag polar $C_D(\theta)$, the lift polar $C_L(\theta)$ as well as the polar for the resulting yaw moment of these two forces $C_T(\theta)$ are presented in Figure 3.

3.1.4. *Equations*

To account for the variation of both the fluid's velocity and orientation depending on z we will integrate (7) and (8) along the $\vec{k}$ axis. This requires to define a cross-sectional area depending on both the heigth z and flow incidence at that height $\theta(z)$. Furthermore the drag, lift and torque coefficients must also be modified to account for this. For the 40-ft container, this can be done by dividing all these coefficients by the air draft or water draft. If H is the total height of the container and I its immersion rate, then the air draft is $(1-I)H$ and the deep draft is IH.

By taking these new parameters into account, we can thus give a detailed formula for all forces and torque (11)–(16).

$$\vec{F}_{D,\text{air}} = \frac{1}{(1-I)H}\int_0^{(1-I)H} \frac{1}{2}\rho_{\text{air}}\, S(\theta_{\text{air}}(z))\, C_D(\theta_{\text{air}}(z))\, |\vec{W(z)} - \vec{V}|^2\, \vec{e}_{\text{air}}(z)\, \mathrm{d}z \tag{11}$$

$$\vec{F}_{D,\text{water}} = \frac{1}{IH}\int_{-IH}^{0} \frac{1}{2}\rho_{\text{water}}\, S(\theta_{\text{water}}(z))\, C_D(\theta_{\text{water}}(z))\, |\vec{U(z)} - \vec{V}|^2\, \vec{e}_{\text{water}}(z)\, \mathrm{d}z \tag{12}$$

$$\vec{F}_{L,\text{air}} = \frac{1}{(1-I)H}\int_0^{(1-I)H} \frac{1}{2}\rho_{\text{air}}\, S(\theta_{\text{air}}(z))\, C_L(\theta_{\text{air}}(z))\, |\vec{W(z)} - \vec{V}|^2\, \vec{e}^{\perp}_{\text{air}}(z)\, \mathrm{d}z \tag{13}$$

$$\vec{F}_{L,\text{water}} = \frac{1}{IH}\int_{-IH}^{0} \frac{1}{2}\rho_{\text{water}}\, S(\theta_{\text{water}}(z))\, C_L(\theta_{\text{water}}(z))\, |\vec{U(z)} - \vec{V}|^2\, \vec{e}^{\perp}_{\text{water}}(z)\, \mathrm{d}z \tag{14}$$

$$\vec{F}_{T,\text{air}} = \frac{1}{(1-I)H}\int_0^{(1-I)H} \frac{1}{2}\rho_{\text{air}}\, S(\theta_{\text{air}}(z))\, C_T(\theta_{\text{air}}(z))\, |\vec{W(z)} - \vec{V}|^2\, \vec{k}\, \mathrm{d}z \tag{15}$$

$$\vec{F}_{T,\text{water}} = \frac{1}{IH}\int_{-IH}^{0} \frac{1}{2}\rho_{\text{water}}\, S(\theta_{\text{water}}(z))\, C_T(\theta_{\text{water}}(z))\, |\vec{W(z)} - \vec{V}|^2\, \vec{k}\, \mathrm{d}z. \tag{16}$$

These formulas are not general and can only be applied to the container (or another object presenting the same geometrical properties).

3.2. *Application to determine the leeway coefficients*

The polar-based method can be applied in two different ways: either by solving (3) and (4) for $\vec{0}$ and looking for a stable equilibrium (the static method) or by integrating these equations over time in order to plot a trajectory (the dynamic method). We will hereafter present both methods.

3.2.1. *Static method*

We assume that both $\vec{W}_{10}$ and $\vec{U}_{\text{ambient}}$ are known in the inertial frame of reference $\mathscr{R}(O,\vec{i},\vec{j},\vec{k})$. Thanks to equations (9) and (10) we can determine $\vec{W}$ and $\vec{U}$. We also assume that the immersion rate I is constant and known.

We then consider the forces $F_i \cdot \vec{i} = (\sum \vec{F}) \cdot \vec{i}$, $F_j \cdot \vec{j} = (\sum \vec{F}) \cdot \vec{j}$ and $T \cdot \vec{k} = \sum \vec{T}$. These forces depend solely on the speed of the object $\vec{V}$ and its heading ϕ (see Figure 2a).

Let us then introduce the tensor $\mathscr{U}$ (17) and its Jacobian matrix $\mathscr{J}$ (18).

$$\mathscr{U} : \begin{pmatrix} V_i \\ V_j \\ \phi \end{pmatrix} \mapsto \begin{pmatrix} F_i(V_i, V_j, \phi) \\ F_j(V_i, V_j, \phi) \\ M(V_i, V_j, \phi) \end{pmatrix} \tag{17}$$

$$\mathscr{J} = \begin{bmatrix} \dfrac{\partial F_i}{\partial V_i} & \dfrac{\partial F_i}{\partial V_j} & \dfrac{\partial F_i}{\partial \phi} \\ \dfrac{\partial F_j}{\partial V_i} & \dfrac{\partial F_j}{\partial V_j} & \dfrac{\partial F_j}{\partial \phi} \\ \dfrac{\partial M}{\partial V_i} & \dfrac{\partial M}{\partial V_j} & \dfrac{\partial M}{\partial \phi} \end{bmatrix}. \tag{18}$$

An equilibrium point is a triplet $(V_{i,\mathrm{eq}}, V_{j,\mathrm{eq}}, \phi_{\mathrm{eq}})$ so that $\mathscr{U}(V_{i,\mathrm{eq}}, V_{j,\mathrm{eq}}, \phi_{\mathrm{eq}}) = (0,0,0)$. Furthermore according to the Hartman–Grobman theorem if the eigenvalues $\lambda_1, \lambda_2, \lambda_3$ of $\mathscr{J}$ at the point $(V_{i,\mathrm{eq}}, V_{j,\mathrm{eq}}, \phi_{\mathrm{eq}})$ are all negative or if their real parts are negative, the equilibrium is stable.

Let us then consider the stable equilibrium $(V_{i,\mathrm{eq,stable}}, V_{j,\mathrm{eq,stable}}, \phi_{\mathrm{eq,stable}})$. The leeway coefficients can be determined by using equations (1) and (2). If we assume that there is no offset (i.e. b_D and b_C are null) we have a direct expression for a_D (19) and a_C (20). This would correspond to a constrained regression in the leeway field method [8].

$$a_D = \frac{DWL}{W_{10}} \tag{19}$$

$$a_C = \frac{CWL}{W_{10}}. \tag{20}$$

The downwind (21) and crosswind leeway (22) can then be expressed depending on only V, U_{amb} and $\vec{W_{10}}$ if we consider Figure 1.

$$DWL = (\vec{V} - \vec{U}_{\mathrm{ambient}}) \cdot \frac{\vec{W_{10}}}{W_{10}} \tag{21}$$

$$CWL = \left| (\vec{V} - \vec{U}_{\mathrm{ambient}}) - DWL \frac{\vec{W_{10}}}{W_{10}} \right|. \tag{22}$$

Alternatively these coefficients can be regarded as coefficients specific to a wind and current condition, thus eliminating the offset problem.

3.2.2. *Dynamic method*

For this method, the drift trajectory is calculated using an explicit Euler scheme (23)–(28). A dissipation coefficient η expressing the percentage of angular velocity lost every second is introduced in (27) to account for angular momentum dissipation caused by the lack of phenomena such as waves and vortices.

$$\dot{x}(t + \mathrm{d}t) = \dot{x}(t) + \frac{F_i \, \mathrm{d}t}{m} \tag{23}$$

$$x(t + \mathrm{d}t) = x(t) + \dot{x}(t + \mathrm{d}t) \, \mathrm{d}t \tag{24}$$

$$\dot{y}(t + \mathrm{d}t) = \dot{y}(t) + \frac{F_j \, \mathrm{d}t}{m} \tag{25}$$

$$y(t + \mathrm{d}t) = y(t) + \dot{y}(t + \mathrm{d}t) \, \mathrm{d}t \tag{26}$$

$$\dot{\phi}(t + \mathrm{d}t) = \dot{\phi}(t)(1 - \eta)^{\mathrm{d}t} + \frac{T \, \mathrm{d}t}{J} \tag{27}$$

$$\phi(t + \mathrm{d}t) = \theta(t) + \dot{\phi}(t + \mathrm{d}t) \, \mathrm{d}t. \tag{28}$$

The results from this method can then be interpreted by assuming that the position reached after a sufficient number of steps is an equilibrium position. Leeway coefficients are then obtained as in the static method.

Alternatively, it is possible to use a variable wind and current forcing and to consider the trajectory as if it were the result of a leeway field experiment. This allows to account for a potential offset.

4. Results

We applied our model to the 40-ft container and tested a vast array of both external parameters (wind and current) and internal parameters (initial conditions, time step and dissipation coefficient) to try and asses its performance. Results from these tests are presented hereafter in

Table 1. The different equilibrium between 0° and 90° and $0 < V_i, V_j < 0.5$ and their stability

Equilibrium point			Eigenvalues of $\mathscr{J}$			Stability
ϕ (°)	V_i (m·s^{-1})	V_j (m·s^{-1})	λ_1 ($\times 10^4$)	λ_2 ($\times 10^4$)	λ_3 ($\times 10^2$)	
0	0.2957	0	−9.062	−8.854	12.40	Unstable
43.57	0.3376	0.2673	2.495	−2.286	11.09	Unstable
56.97	0.1988	0.1608	$-2.549+3.459i$	$-2.549-3.459i$	2.757	Unstable
79.88	0.1854	0.08699	$-2.464+1.691i$	$-2.464-1.691i$	−1.962	Stable
90.00	0.2957	0	−1.203	1.680	3.766	Unstable

three independent subsections. The first section focuses on the determination of the leeway coefficients using the polar-based method and their comparison to results from the leeway field method. In the second section we examine other characteristics of the leeway that have been experimentally documented. In the last section we apply our model to determine drift trajectory directly.

4.1. *Determination of the leeway coefficient for a 40-ft container at 70% of immersion*

4.1.1. *Application of the static method*

We applied the static method on the 40-ft container at 70% immersion ($I = 0.7$) with no ambient current and a west wind (positively along the x axis) of 10 m·s^{-1}. Considering the symmetries of the problem, we limited our study to $\phi = [0°; 90°]$. Indeed, since the container is invariant by a 180° rotation we can limit ourselves to [0°; 180°]. As the problem would remain the same if it were mirrored along the i axis we can once again restrict the range of study to [0°; 90°]. In this range five equilibria were found, they are presented in Figure 4.

The Jacobian matrix $\mathscr{J}$ (18) was then determined and diagonalised for each of these equilibria. Only the one at 79.88° had all three of its eigenvalues strictly negative and is thus stable. Since we considered a west wind, this corresponds to an angle of incidence $\theta_{W_{10}}$ of 10.12° for the 10-m wind. The others all had a λ_3 positive which suggests that they are unstable along ϕ. The results are compiled in Table 1.

These equilibria can then be mirrored along the i axis to account for the symmetry in both wind and current and so the transformation $(V_i, V_j, \phi) \mapsto (V_i, -V_j, 180 - \phi)$ gives us the corresponding equilibrium on [90°; 180°]. Accounting for the symmetry of the container, the transformation $(V_i, V_j, \phi) \mapsto (V_i, V_j, \phi + 180)$ can then be applied and so the equilibria on [180°; 360°] are known. All equilibria determined this way retain the same stability as their original counterpart. In a more complex case with a current that is neither null nor collinear to the wind and an object presenting no symmetry, the study must be conducted for all angles ϕ.

This way, we found four stable equilibria corresponding to a heading of 79.9° with leeway coefficients $a_D = 1.854\%$ and $a_C = 0.8699\%$ (Figure 4d), its mirror at 100.1° with $a_D = 1.854\%$ and $a_C = -0.8699\%$ and their respective symmetric at 259.9° and 280.1° with the same respective leeway coefficients. There are thus two distinct stable equilibria which have the same downwind coefficient, but opposite crosswind coefficient. This configuration with a crosswind leeway that can be either to the "left" or the "right" of the downwind leeway and crosswind leeway coefficients that are thus positive or negative is coherent with field observation [8].

However, since these coefficients were established using only one wind speed, their values cannot be compared directly with previous studies. We need to either repeat this operation for different wind speed or use another method.

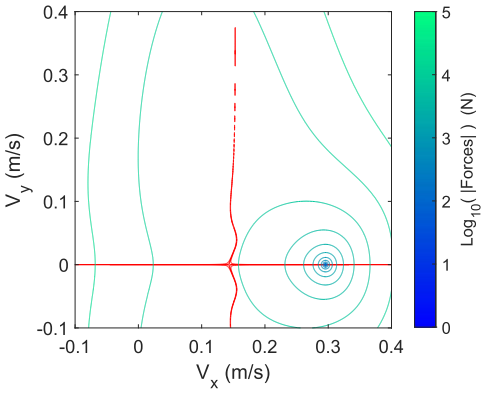

(a) Heading = 0°

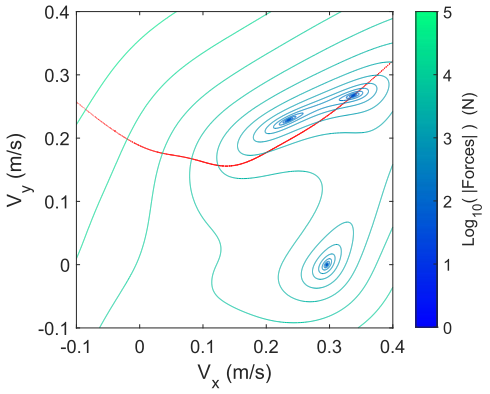

(b) Heading = 43.6°

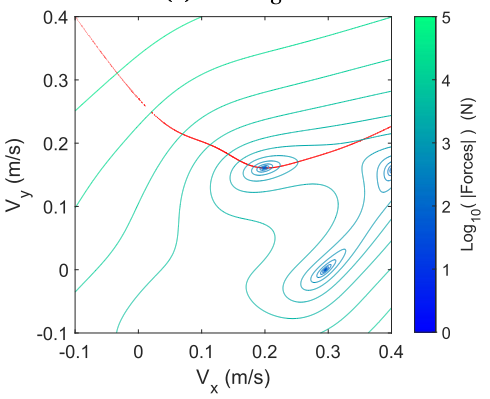

(c) Heading = 57°

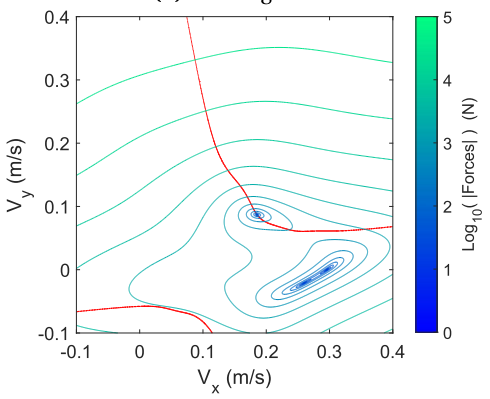

(d) Heading = 79.9°

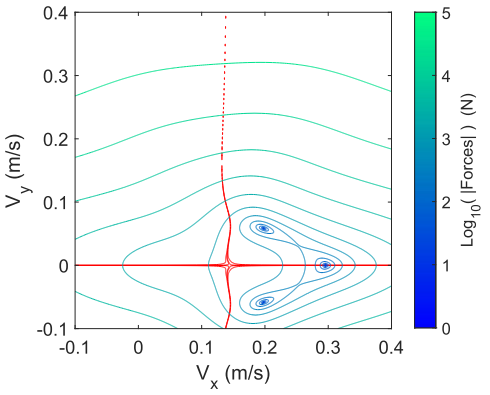

(e) Heading = 90°

Figure 4. Equilibria for the 40-feet containers in a 10 $m \cdot s^{-1}$ west wind. Each sub-figure corresponds to a different heading of the container; norm of the forces exerted on the container are plotted as blue-green isolines on a logarithmic scale and points of null momentum are plotted in red.

Table 2. Comparison of leeway coefficients a, a_D, a_C, and their associated standard deviation σ and coefficient of determination r^2 between the results from Breivik *et al.* [8] and the polar-based model

	Leeway speed			*DWL*			*CWL*		
	a (%)	σ (cm·s^{-1})	r^2	a_D (%)	σ (cm·s^{-1})	r^2	a_C (%)	σ (cm·s^{-1})	r^2
Breivik *et al.*	2.00	3.03	0.71	1.96	3.08	0.83	0.02	2.65	−0.11
Our model	1.80	2.12	0.914	1.58	2.38	0.875	0.856	0.330	0.987

4.1.2. *Application of the dynamic method*

The static method, though accurate, is relatively tedious. As such the dynamic method has been preferred for it allows us to more easily test various wind and current conditions in order to compare it to the results from Breivik *et al.* [8].

We first verified that the results from both methods coincide for a wind speed of 10 m·s^{-1}. This confirmed that this model did indeed reach the equilibrium point after a sufficient number of iterations.

We then performed 100 different runs, each with a different wind and current condition. The wind conditions were evenly distributed between 0.1 and 11.1 m·s^{-1} in order to replicate the field conditions encountered by Breivik *et al.* [8]. The ambient current was evenly distributed between 0 and 0.5 m·s^{-1} with a random orientation regarding the wind. Each run consisted of 7200 steps with a time step of $\mathrm{d}t = 1$ s. After 7200 steps both the speed and the heading were remaining constant, indicating that the equilibrium had been reached. The speed of the last step of the run was thus considered to be the equilibrium speed for the wind and current conditions of the said run. This equilibrium speed was then turned into a downwind and crosswind leeway via (21) and (22). The results of the 100 runs are presented in Figure 5 and Table 2 where they are compared with the results from the scaled-down 40-ft container obtained by Breivik *et al.* [8].

We chose to use constrained linear regression to eliminate any offset which would indicate the existence of the leeway even in the absence of wind. This is possible because an apparent wind can exist as long as the speed over ground of the object is not null, and also because leeway is defined as the motion of the object induced not only by wind but also by waves. We however still found it problematic as it is then impossible to determine the downwind direction.

As can be seen in Table 2, the coefficients a and a_D are consistent from one method to another. The coefficient a_C presents for its part significant differences between the two approaches. Since the crosswind leeway is highly impacted by variations in heading, a small error on this part can be greatly amplified when considering a_C. As such, the angle step of 15° we used to compute the polars might be too important. Furthermore the coefficient given by Breivik *et al.* [8] for the modelled 40-ft container exhibits a high uncertainty on the linear regression and it is thus difficult to conclude. It is interesting to note that for both the leeway and downwind leeway the relation to wind speed appears not to be linear but rather a parabola which is in contradiction with existing studies. A possible explanation for this lies is the way the surface current was accounted for in our method, as we did not include it in the ambient current.

4.2. *Determination of others leeway behaviours*

In addition to determining the leeway coefficients, we tried to see whether or not our model could reproduce other behaviours and properties that have been observed during field studies.

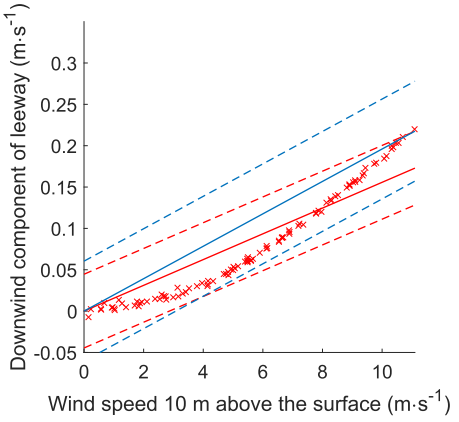

(a) Downwind component of the leeway.

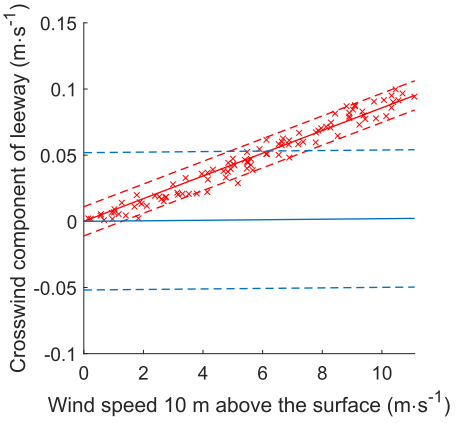

(b) Crosswind component of the leeway.

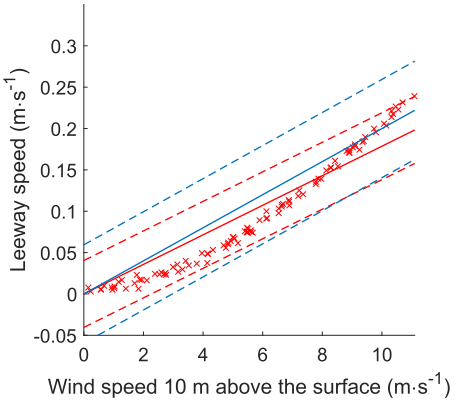

(c) Leeway speed.

Figure 5. DWL and CWL speed in m·s^{-1} for various conditions of wind and current. The leeway rate (solid) and associated 95% confidence interval (dashed) found by Breivik *et al.* [8] for a constrained linear regression are plotted in blue ; equilibrium speed for different conditions (crosses) and leeway rate (solid) obtained via our model are plotted in red.

4.2.1. *Variation of the leeway as a function of the wind–current angle*

By plotting the leeway rate as a function of the wind–current angle as illustrated in Figure 6, we can note that there appears to be a dependency between these two parameters. This dependency was also found experimentally by Cabioc'h and Aoustin [13] although they did not give an explanation for it.

While the wind–current angle β does not appear explicitly in our model, it appears implicitly as $\theta_{\text{water}} = \theta_{\text{air}} - \beta$. As such, it has a direct impact on C_{water} and thus on the equilibrium.

4.2.2. *Variation of the leeway as a function of the immersion rate*

A second phenomenon reported in the literature is the variation of the leeway as a function of the immersion rate which has been discussed in several articles [12, 13]. The formula (29) based on mechanical considerations has been proposed by Daniel *et al.* [12] with r the density ratio of

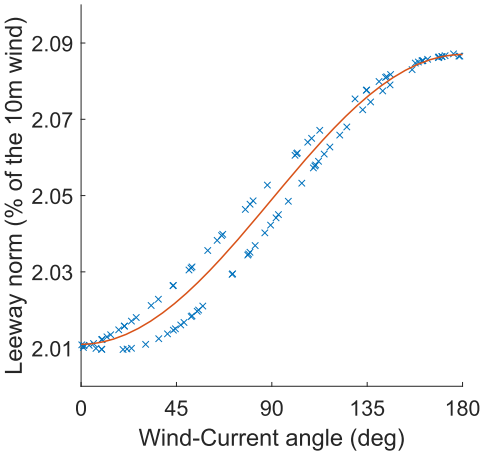

Figure 6. Drift speed versus angle wind current. Blue x represents results from separate runs and a cosines regression is plotted in red.

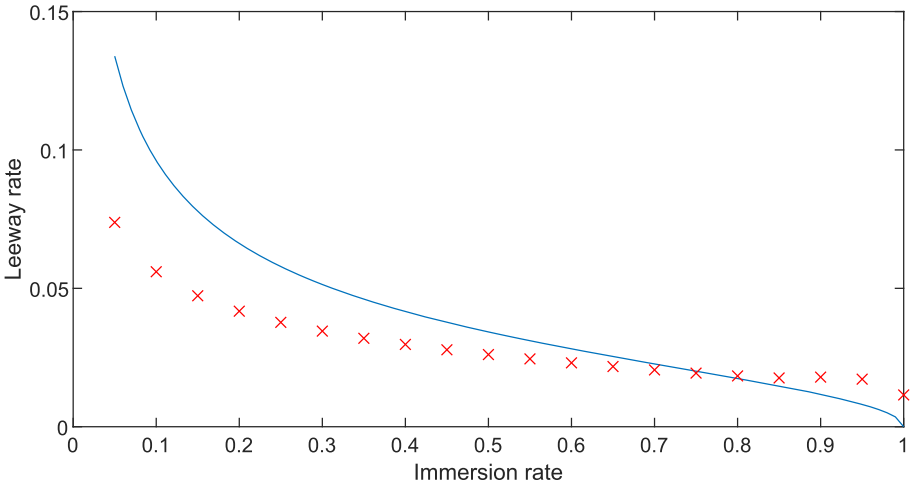

Figure 7. Variation of the leeway depending on I. Results from the polar-based method are plotted with red x and Daniel *et al.* formula (29) [12] is plotted with a solid blue line.

air and water, and I the immersion rate.

$$L(I) = \frac{100 - I - \sqrt{rI(100 - I)}}{100 - (1 + r)I}. \tag{29}$$

This formula can then be compared with the results hailing from our model as illustrated in Figure 7. The values we used for this comparison were obtained for $W_{10} = 10$ m·s^{-1} as it is at this point that we observed the closest match between our model and the values of Breivik *et al.* [8].

While both figures coincide for an immersion rate of around 75%, large discrepancies appear for extreme values. These differences arise from the fact that the formula proposed by Daniel *et al.* [12] does not take surface current into account, and thus the leeway is equal to zero for an immersion rate of 100%. However, in our model, a drifting container is still influenced by the wind through the surface current.

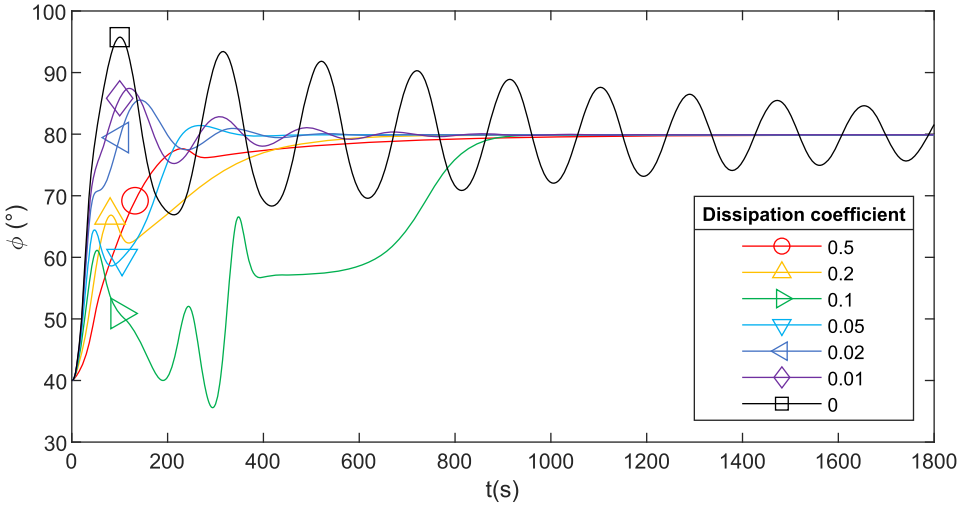

Figure 8. Variation of the heading over time depending on the dissipation coefficient for otherwise identical initial conditions.

The second source of difference stems from the fact that the Daniel *et al.* [12] formula does not account for the variation of the coefficients C and S depending on the angle of attack of the flow. This means that they are taken to be equal and are therefore simplified to leave only a ratio of immersion between the emerged part and the submerged part, as well as a ratio of density between air and water. However, at equilibrium in the general case the relative wind and the relative current do not have the same direction, which partly explains the differences observed between the two models.

4.3. *Use of the direct method to plot trajectories*

As stated previously, the direct method can be employed to directly compute an estimated trajectory. This however raises issues concerning the choice of the dissipation coefficient and the precision of the model.

4.3.1. *Impact of the dissipation coefficient*

The dissipation coefficient introduced in (27) does not interfere with the equilibrium point, however it can have a significant impact on the trajectory as depicted in Figure 8. If the system is over-damped (dissipation coefficient of more than 20%) there is no oscillation, while if the system is clearly under-damped (dissipation coefficient of less than 5%) the system can oscillate for several minutes before it finally reaches the equilibrium. Coefficients that lie between these two values can result in curves that are quite peculiar as they do not resemble those from a simple damped oscillator. For these values the non-linear nature of the system is quite clear and the influence of non-stable equilibrium points can be assumed. In particular, inflexion points appear around 43° and 58° which precisely coincide with non-stable equilibrium points in Table 1.

4.3.2. *Existence of dynamic equilibrium*

By conducting further simulations with dissipation coefficient in the critical range (5%–20%) we found that equilibrium that are not restricted to a single point in the phase space (V_x, V_y, ϕ) exists for specific conditions. Six different runs for a dissipation coefficient of 15% and fine-tuned initial parameters are depicted in Figure 9 to illustrate various effects.

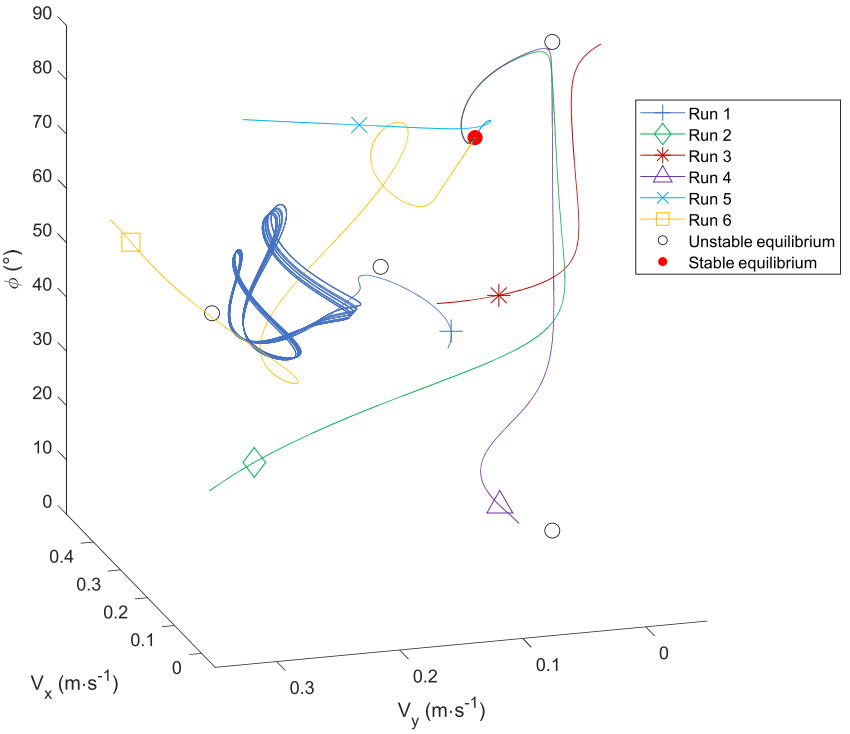

Figure 9. Trajectories in the phase space (V_x, V_y, ϕ) of six different runs with varying initial conditions.

The run numbers 2, 4, 5 and 6 all converged toward the stable equilibria at 79.88° previously determined (see Table 1). They were however differently impacted by the various unstable equilibrium. Run number 5 directly converged toward the stable equilibrium, while run 2 and 4 first converged toward the unstable equilibrium at 90°. Run number 6 had a somewhat more convoluted trajectory, though it seems that it was influenced by several unstable equilibria.

The run number 3 converged toward the equilibrium at 100.12° which is the mirror of the equilibrium at 79.88° but is out of bounds in Figure 9. As such it exhibited a comportment that can be assimilated to a jibe since its crosswind speed changed sign at some point. It is however not a true jibe as it did not go from one stable equilibrium to another.

Finally the run number 1 (see Figure 10 for an enlarged version) is unique in the fact that it did not converge toward an equilibrium point but rather looped around two unstable equilibria. Furthermore unlike the other equilibria it exhibited a chaotic behaviour as even a slight perturbation of the initial conditions results in a significant difference over time. This is illustrated in Figure 11 for the heading. The initial heading was increased by 10^{-5} degrees and compared over time to its original value. For more than 10,800 iterations (3 h of time as we used $\mathrm{d}t = 1$ s) the deviation was not noticeable (less than 0.2°), but over the next 10,800 iterations the divergence had reached more than 10°. This is characteristic of a chaotic behaviour. In addition, the trajectory appears to be a fractal (see Figure 12), which, in addition to the chaotic behaviour would indicate that we are in presence of a strange attractor. While we believe this to be strictly a consequence of our oversimplified model (as such behaviour has never been observed for relatively permanent conditions of wind and current) it is still of interest as it highlights the dependence of the model to initial conditions. Since such initial conditions are hardly ever known in operatiing conditions, much less to such a precision, a stochastic approach remains necessary.

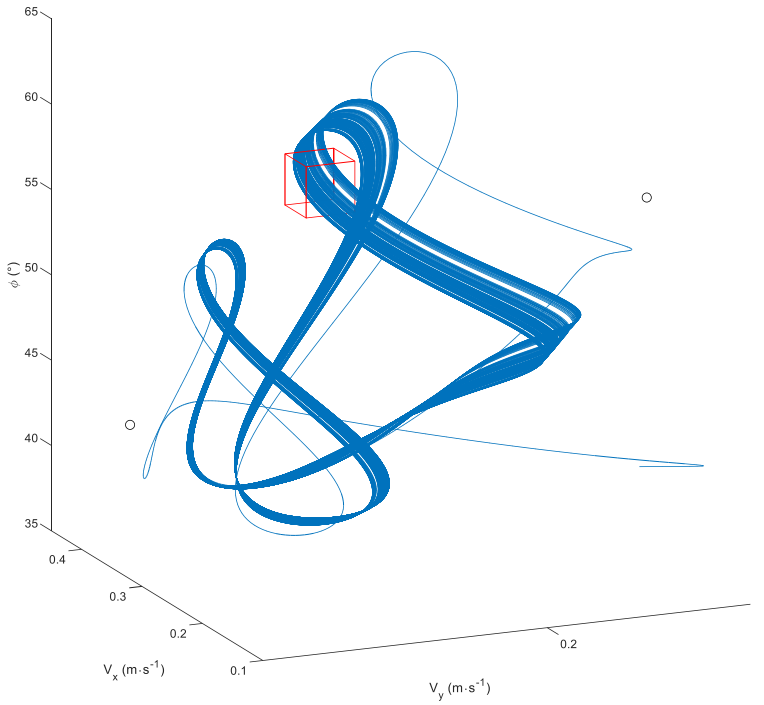

Figure 10. A zoom on the trajectory of run number 1. The red box indicates the position of Figure 12.

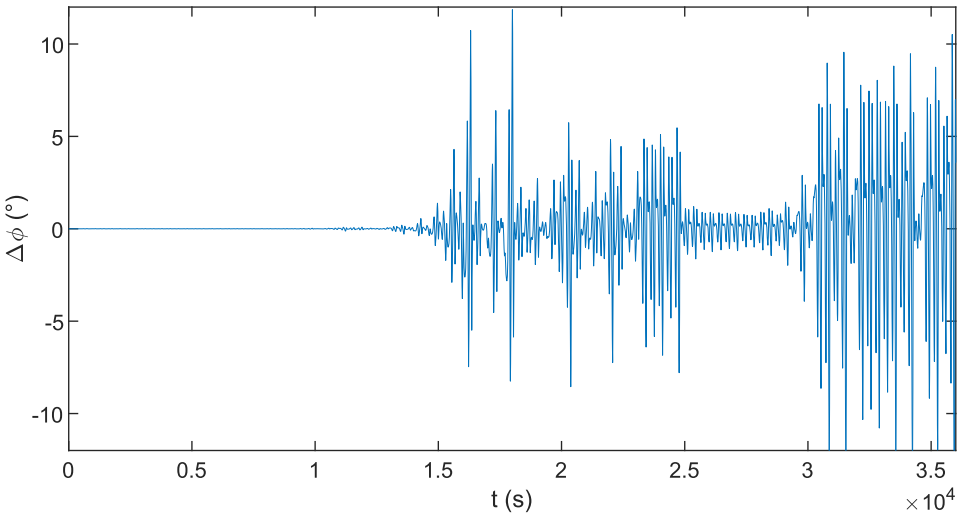

Figure 11. Evolution in the difference in heading over time between two trajectories following the same dynamic equilibrium, with only a difference of 10^{-5} degrees in the initial heading.

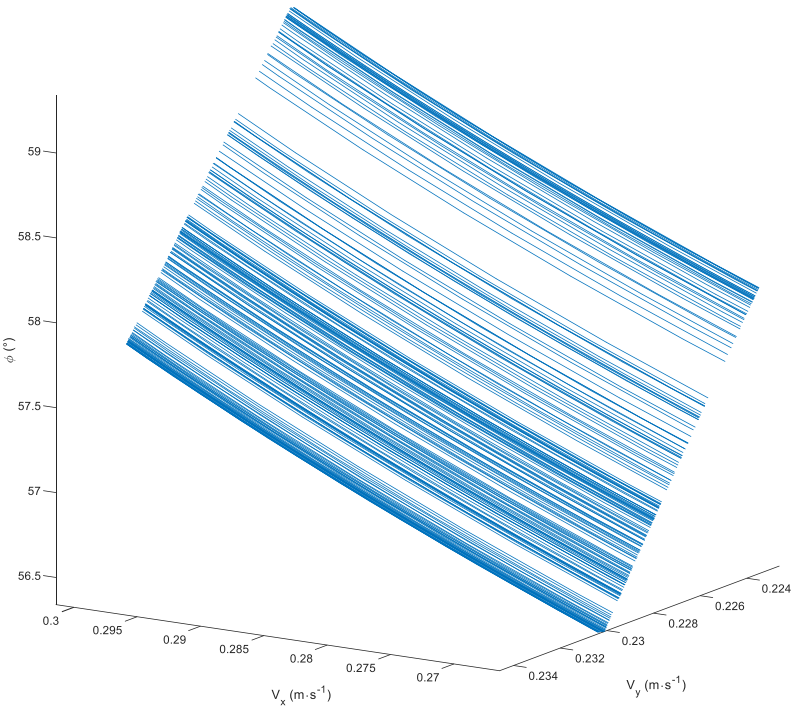

Figure 12. Fine structure of a part of run number one's trajectory.

5. Conclusion

We have given an overview of a new method for determining the leeway coefficients of drifting objects. This new method boils down to the use of polars of drag, lift and torque to solve Newton's second law of motion. Simple formulas to derive a wind and current profile from the 10-m wind and ambient current were presented. Two methods of exploiting the results from this model to obtain the leeway coefficients were given.

We applied this new method to the example of the 40-feet container. We found a downwind leeway of 1.58% of the 10-m wind and a crosswind leeway of 0.86%. The downwind leeway coefficient is within 2σ from the one obtained with the leeway field method. The crosswind leeway coefficient however appears to be too high. Since this coefficient bears a high uncertainty in the leeway field method it is difficult to conclude. The model successfully replicated the dependency on the wind–current angle and the immersion rate of the leeway.

While we consider the first results promising, some improvements are to be made. A more general way of accounting for wind and current profile must be devised in order to allow the use of this method for different classes of objects. If the dynamic method is to be used, it appears necessary to devise a way to get an approximation of the dissipation coefficient. This could be done either by means of CFD, or through experiments on scaled-down models. It will also be necessary to implement a higher-order algorithm to solve the differential equations (such as a Runge–Kutta scheme). In the long term it will also be necessary to gradually integrate the phenomena which have hitherto been considered negligible, such as the effect of waves or vortices. Field studies need to be conducted to validate this new model since the heading of the object is critical but was not previously monitored. Finally, the question of uncertainties must be addressed to better evaluate their propagation throughout the model.

Conflicts of interest

The authors declare no competing financial interest.

Dedication

The manuscript was written through contributions of all authors. All authors have given approval to the final version of the manuscript.

Acknowledgments

This work is part of the project OSCAR which was launched and financed by the "Direction des Affaires Maritimes (DAM)" (French Directorate for Maritime Affairs). We would like to thank the "Sous-direction des Services Maritimes et du Contrôle (SMC)" (DAM's Maritime Service and Enforcement Branch) and in particular Hervé Guichard (IT project manager to the SMC director) whose comments greatly helped us along the way.

References

[1] P. Daniel, "Le modèle MOTHY et ses évolutions", in *Journée de discussions techniques du Cedre*, Cedre, Brest, 2019 (fr), http://wwz.cedre.fr/content/download/10220/file/pierre-daniel-mothy-2019.pdf.

[2] L. E. Hillier, "Validating and improving the Canadian coast guard search and rescue planning program (CANSARP) ocean drift theory", 2008, Master's thesis, Memorial University of Newfoundland, https://research.library.mun.ca/9414/ (accessed 25 October 2021).

[3] T. M. Kratzke, L. D. Stone, J. R. Frost, "Search and rescue optimal planning system", in *2010 13th International Conference on Information Fusion*, IEEE, Edinburgh, 2010 (en), http://ieeexplore.ieee.org/document/5712114/ (accessed 22 October 2021).

[4] Ø. Breivik, A. A. Allen, C. Maisondieu, J. C. Roth, "Wind-induced drift of objects at sea: The leeway field method", *Appl. Ocean Res.* **33** (2011), no. 2, p. 100-109 (en), https://www.sciencedirect.com/science/article/abs/pii/S014111871100006X (accessed 12 February 2020).

[5] Ø. Breivik, A. A. Allen, C. Maisondieu, M. Olagnon, "Advances in search and rescue at sea", *Ocean Dyn.* **63**, no. 1, p. 83-88 (en), http://link.springer.com/10.1007/s10236-012-0581-1 (accessed 26 August 2021).

[6] A. A. Allen, J. V. Plourde, "Review of leeway: field experiments and implementation", Tech. report, Coast Guard Research and Development Center Groton CT, 1999, https://apps.dtic.mil/sti/citations/ADA366414 (accessed 19 April 2022).

[7] A. A. Allen, "Leeway divergence", Tech. report, Coast Guard Research and Development Center Groton CT, 2005, https://apps.dtic.mil/sti/citations/ADA435435 (accessed 19 April 2022).

[8] Ø. Breivik, A. A. Allen, C. Maisondieu, J.-C. Roth, B. Forest, "The leeway of shipping containers at different immersion levels", *Ocean Dyn.* **62** (2012), no. 5, p. 741-752 (en), http://link.springer.com/10.1007/s10236-012-0522-z (accessed 12 February 2020).

[9] C. Maisondieu, B. Forest, "Container drift assessment - iroise sea experiment. sar-drift project", 2008, Campaign Report ERT/HO 08-R04HO08, Ifremer, https://archimer.ifremer.fr/doc/00238/34970/.

[10] Ø. Breivik, A. A. Allen, "An operational search and rescue model for the Norwegian Sea and the North Sea", *J. Mar. Syst.* **69** (2008), no. 1–2, p. 99-113 (en), http://arxiv.org/abs/1111.1102 (accessed 16 March 2021).

[11] A. Allen, J.-C. Roth, C. Maisondieu, O. Breivik, B. Forest, "Field determination of the leeway of drifting objects", Tech. Report 17, Norwegian Meteorological Institute, 2010, https://archimer.ifremer.fr/doc/00254/36492/ (accessed 19 April 2022).

[12] P. Daniel, G. Jan, F. Cabioc'h, Y. Landau, E. Loiseau, "Drift modeling of cargo containers", *Spill Sci. Technol. Bull.* **7** (2002), no. 5–6, p. 279-288 (en), https://www.sciencedirect.com/science/article/abs/pii/S1353256102000750 (accessed 12 February 2020).

[13] F. Cabioc'h, Y. Aoustin, "Criteria for decision making regarding response to accidentally spilled chemicals in packaged form: Hydrodynamic aspects", *Spill Sci. Technol. Bull.* **4** (1997), no. 1, p. 7-15 (en), https://www.sciencedirect.com/science/article/abs/pii/S1353256197000297 (accessed 09 July 2020).

[14] B. A. Brushett, A. A. Allen, V. C. Futch, B. A. King, C. J. Lemckert, "Determining the leeway drift characteristics of tropical Pacific Island craft", *Appl. Ocean Res.* **44** (2014), p. 92-101 (en), https://linkinghub.elsevier.com/retrieve/pii/S0141118713001004.

[15] M. Le Boulluec, B. Forest, E. Mansuy, "Steady drift of floating objects in waves: experimental and numerical investigation", in *Ocean Engineering; Offshore Renewable Energy*, vol. 4, ASMEDC, Estoril, Portugal, 2008 (en), https://asmedigitalcollection.asme.org/OMAE/proceedings/OMAE2008/48210/321/324969, p. 321-328.

[16] Q. Li, Y. Nihei, T. Nakashima, Y. Ikeda, "A study on the performance of cascade hard sails and sail-equipped vessels", *Ocean Eng.* **98** (2015), p. 23-31 (en), https://www.sciencedirect.com/science/article/abs/pii/S0029801815000268 (accessed 08 November 2021).

[17] L. Thiebaud, A.-L. Tiberi-Wadier, Y. Beaudouin, "Analyse de données de vent en Europe pour caractériser le potentiel de l'éolien en mer", in *XVèmes Journées Nationales Génie Côtier - Génie Civil*, Paralia CFL, La Rochelle, 2018 (fr), https://www.paralia.fr/jngcgc/15_67_thiebaud.pdf (accessed 17 August 2020).

[18] F. Ardhuin, L. Marié, N. Rascle, P. Forget, A. Roland, "Observation and estimation of lagrangian, stokes, and Eulerian currents induced by wind and waves at the sea surface", *J. Phys. Oceanogr.* **39** (2009), no. 11, p. 2820-2838 (en), https://journals.ametsoc.org/view/journals/phoc/39/11/2009jpo4169.1.xml (accessed 09 July 2020).

[19] J. Röhrs, K. H. Christensen, L. R. Hole, G. Broström, M. Drivdal, S. Sundby, "Observation-based evaluation of surface wave effects on currents and trajectory forecasts", *Ocean Dyn.* **62** (2012), no. 10–12, p. 1519-1533 (en), http://link.springer.com/10.1007/s10236-012-0576-y (accessed 16 September 2021).

[20] K. E. Kenyon, "Stokes drift for random gravity waves", *J. Geophys. Res.* **74** (1969), no. 28, p. 6991-6994 (en), https://agupubs.onlinelibrary.wiley.com/doi/abs/10.1029/JC074i028p06991 (accessed 07 September 2020).

[21] S. Kaidi, H. Smaoui, P. Sergent, "CFD investigation of mutual interaction between hull, propellers, and rudders for an inland container ship in deep, very deep, shallow, and very shallow waters", *J. Waterw. Port, Coast. Ocean Eng.* **144** (2018), no. 6, article no. 04018017 (en), https://www.researchgate.net/publication/326982505_CFD_Investigation_of_Mutual_Interaction_between_Hull_Propellers_and_Rudders_for_an_Inland_Container_Ship_in_Deep_Very_Deep_Shallow_and_Very_Shallow_Waters.

[22] I. Razgallah, S. Kaidi, H. Smaoui, P. Sergent, "The impact of free surface modelling on hydrodynamic forces for ship navigating in inland waterways: water depth, drift angle, and ship speed effect", *J. Mar. Sci. Technol.* **24** (2019), no. 2, p. 620-641 (en), http://link.springer.com/10.1007/s00773-018-0566-y.